On the Orientational Analysis of Boolean Fibres from Digital Images

SALME KÄRKKÄINEN*, EVA B. VEDEL JENSEN**
DOMINIQUE JEULIN***

*Department of Mathematics and Statistics, University of Jyväskylä, P.O. Box 35 (MaD) FIN-40351 Jyväskylä, Finland
email: samk@maths.jyu.fi, tel: +358 14 260 2984, fax: +358 14 260 2981
**Laboratory for Computational Stochastics, Department of Mathematical Sciences, Ny Munkegade, DK-8000 Aarhus C, Denmark
email: eva@imf.au.dk, tel: +45 89 42 35 18, fax: +45 86 13 17 69
***Centre de Morphologie Mathématique, Ecole Nationale Supérieure des Mines de Paris, 35 rue St Honore, F77300 Fontainebleau, France
email: Dominique.Jeulin@cmm.ensmp.fr, tel: 33 1 64 69 47 95, fax: 33 1 64 69 47 07

Abbreviated running title: Orientational Analysis of Boolean Fibres
Keywords: Boolean model, dead leaves model, digital image, fibre process, point intensity, rose of directions, scaled variogram, simulation, stereology.

Summary

The orientational characteristics of fibres in digital images are studied. The fibres are modelled by a planar Boolean model whose typical grain is a thickened (coloured) fibre. The aim is to make stereological inference on the rose of directions of unobservable central fibres from observations made on a digital image of the thick fibres. For central fibres, the relation between the rose of directions and the point intensity, observed on a sampling line, is known. We derive, under regularity conditions, the relation between the unobservable point intensity and the scaled variogram observed on the line in a binary and a greyscale image. Using such a relation, it is possible to draw inference about the rose of directions from the scaled variogram which is easy and fast to determine in a digital image.

1 Introduction

The estimation of the orientation distribution of planar fibres from intersection counts along sampling lines is a well-studied subject in the stereological literature, cf. e.g. Hilliard (1962), Mecke & Stoyan (1980), Mecke (1981). Methods of estimating the orientation distribution also exist in non-ideal situations where fibres overlap due to thickness and are observed in digital greyscale images. In Serra (1982, p. 467) the orientation distribution is obtained from a greyscale image, using sequential thresholding of grey levels. At each threshold, counts of intercepts along sampling lines are determined. Greyscale images are also considered in Erkkilä *et al.* (1998) where the estimate of the distribution is based on an approximation of the gradient direction in each pixel. In Molchanov & Stoyan (1994), a method based on empirical capacity functionals is developed for binary images.

In the present paper we develop a method for estimating the orientation distribution based on the scaled variogram which is easy and fast to calculate, without thresholding. The method is intended for biological and industrial fibrous materials which can be modelled by a planar Boolean model whose typical grain is a thickened coloured fibre. The model is the so-called dead leaves random functions model with finite time, resulting in a greyscale image partially covered by the fibres, cf. Jeulin (1989). A binary image is a special case.

The focus is on the estimation of the rose of directions $\mathcal{R}$ of the unobservable central fibres (spines) from orientational characteristics of the thickened fibres observed on sampling lines L_β with angles β relative to a fixed direction. If the central fibres were detectable, the well-known method of estimating $\mathcal{R}$ from the rose of intersections P_L^0 observed on lines could be used, cf. e.g. Mecke & Stoyan (1980). However, since the fibres are thickened and may overlap, the central fibres and thus the point intensity $P_L^0(\beta)$ on L_β are not identifiable; instead, the point intensity $P_L^1(\beta)$ between the boundary of the thickened fibres and the line L_β may be observed. The relation between $P_L^0(\beta)$ and $P_L^1(\beta)$ is derived, and it is shown that the two quantities are proportional if the extent of the fibres is much larger than their thickness. In such cases, the orientation distribution $\mathcal{R}$ can be estimated using the rose of intersections P_L^1 instead of P_L^0 without knowing the thickness of the fibres.

In digital binary images $P_L^1(\beta)$ cannot be observed. Instead, the scaled variogram $V_L(d,\beta)$, where d is the distance between observation points on the sampling line L_β, may be determined. In the binary case the scaled

variogram $V_L(d,\beta)$ approximates $P_L^1(\beta)$ when d is sufficiently small; in the grey level case the scaled variogram $V_{L_{dl}}(d,\beta)$ is approximately proportional to $P_L^1(\beta)$, cf. Jeulin (2000). In practice, it may be a problem that arbitrarily small distances d are not available in a digital image. In the present paper, a refined relation between $V_L(d,\beta)$ and $P_L^1(\beta)$ is derived. This result can also be used for a greyscale image if segmentation into a binary image is possible.

The paper is organized as follows. In Section 2 the set-up for thickened fibres is introduced. The relation between the point intensity $P_L^0(\beta)$ and the rose of directions $\mathcal{R}$ of the central fibres is also given. In Section 3 the general relation between the point intensities $P_L^0(\beta)$ and $P_L^1(\beta)$ is derived for Boolean fibres. Section 4 shows the precise form of this relation for two specific examples of Boolean fibres. In Section 5 the refined relation between the point intensity $P_L^1(\beta)$ and the scaled variogram $V_L(d,\beta)$, observed in a binary digital image, is derived, while the case of greyscale images is discussed in Section 6. Simulation examples are considered in Section 7. In Section 8 the effect of using digital lines instead of continuous lines is briefly studied. In Section 9, the main results of the paper are summarized.

2 The set-up

Let us consider a marked point process $\Psi = \{[x_i;(\Gamma_i,\Xi_i)]\}$ where the points x_i constitute a point process in $\mathbb{R}^2$ and the marks (Γ_i,Ξ_i) are random compact sets in $\mathbb{R}^2$ such that $\Gamma_i \subseteq \Xi_i$, cf. e.g. Matthes (1963) and Stoyan *et al.*, (1995). The marked point process is assumed to be stationary, i.e. $\{[x_i+x;(\Gamma_i,\Xi_i)]\}$ has the same distribution as $\{[x_i;(\Gamma_i,\Xi_i)]\}$ for all $x \in \mathbb{R}^2$. Each Γ_i is a fibre, i.e. a smooth, simple curve of finite length. Furthermore,

$$\Gamma = \cup_{i=1}^{\infty}(x_i + \Gamma_i)$$

is a fibre process, such that the length of $\Gamma \cap B$ is finite for all compact subsets B of $\mathbb{R}^2$. Fibre processes have been introduced in Mecke & Stoyan (1980). The set Ξ_i, containing Γ_i, can in principle be an arbitrary compact set but in the applications we have in mind Ξ_i is a 'thickened' version of Γ_i. The Γ_i's are also called central fibres. A simple example of Ξ_i is a circle-dilated fibre

$$\Xi_i = \Gamma_i \oplus B(O,r),$$

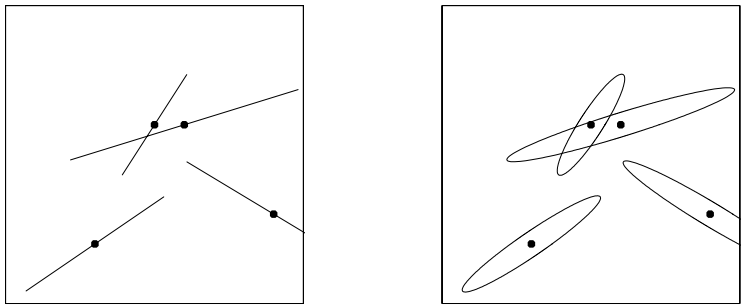

(a) (b)

Figure 1: Illustration of the set-up. a) The central fibres $x_i + \Gamma_i$ are here line segments. b) The thick fibres $x_i + \Xi_i$ are flat ellipses centred at x_i.

where $B(O,r)$ is a circular disk with centre O and radius r (chosen small compared to the radii of curvature of the Γ_i's). We let

$$\Xi = \cup_{i=1}^{\infty}(x_i + \Xi_i)$$

be the union of thick fibres. In Figure 1 the set-up is illustrated. Since the marked point process Ψ is stationary, the fibre process Γ and the process of thick fibres Ξ are also both stationary. If Ψ is isotropic, then Γ and Ξ are both isotropic.

In the present paper we study the problem of making inference about the orientation of the unobservable central fibres Γ from observation of the orientation of the thick fibres Ξ. The orientational characteristic of any stationary fibre process, in particular Γ, can be described by the so-called rose of directions $\mathcal{R}$ which is a distribution on $[0,\pi)$. For $x \in \Gamma$, let $\alpha(x) \in [0,\pi)$ be the angle that the tangent to Γ at x makes with a fixed axis. Then, if ν_1 and ν_2 denote length and area, respectively, we have for Borel sets $B \subseteq \mathbb{R}^2$ and $D \subseteq [0,\pi)$,

$$E\nu_1\{x \in \Gamma \cap B : \alpha(x) \in D\} = L_A \nu_2(B)\mathcal{R}(D),$$

where L_A is the length intensity of the fibre process. Note that $\mathcal{R}(D)$ is the ratio between the mean length of fibre pieces in B having tangent angles in D and the mean total fibre length in B.

In paper fibre technology, the elliptic distribution is often used as a model

for $\mathcal{R}$, compare with Forgacs & Strelis (1963). The density is

$$f_{\mathcal{R}}(\alpha;\kappa,\tau) = \frac{c}{\sqrt{1-\kappa^2\cos^2(\alpha-\tau)}}, \qquad 0 \le \alpha < \pi, \tag{1}$$

with orientation parameters $\kappa \in (0,1)$, $\tau \in [0,\pi)$, and normalizing constant c. Here κ, called the strength, describes deviation from the circular model ($\kappa = 0$) and τ, called the critical direction, is the preferred direction of the fibres. Our reasoning is not restricted to this particular model (1); alternative choices of orientation distribution can be applied as well.

Another orientational characteristic, the so-called rose of intersections $P_L^0(\beta) : [0,\pi) \to [0,\infty)$, is related to $\mathcal{R}$. The quantity $P_L^0(\beta)$ is the intensity of the process of intersection points between the fibre process Γ and a line L_β with angle β relative to the x_1-axis. The two orientational characteristics are related by

$$P_L^0(\beta) = L_A \int_0^\pi |\sin(\alpha-\beta)| \mathcal{R}(d\alpha), \tag{2}$$

see Hilliard (1962), Mecke & Stoyan (1980), Mecke (1981). Similar formulas can also be found in Forgacs & Strelis (1963).

3 From the point intensity $P_L^0(\beta)$ to the point intensity $P_L^1(\beta)$

Assume that the points $\{x_i\}$ of the marked point process Ψ is a stationary Poisson point process in $\mathbb{R}^2$ with intensity λ and $\{(\Gamma_i,\Xi_i)\}$ are independent and identically distributed and independent of $\{x_i\}$. Then both Γ and Ξ are Boolean models (Matheron, 1967; 1972). Below, we let (Γ_0,Ξ_0) be typical thin and thick fibres from the common distribution of $\{(\Gamma_i,\Xi_i)\}$. Then, we have $L_A = \lambda E\nu_1(\Gamma_0)$. For simplicity we assume that Γ_0 and Ξ_0 are convex. In particular, it is assumed that Γ_0 is a line segment. It should be noted, however, that the results can be extended to the non-convex case.

Let us consider the Boolean models Γ and Ξ intersected by the sampling line L_β. On the line, the point processes $L_\beta \cap \Gamma$ and $L_\beta \cap \partial\Xi$, where $\partial\Xi$ is the boundary of the union of thick fibres, are both Boolean models, cf. Matheron (1975, p. 140). In this section we relate the point intensities $P_L^0(\beta)$ of $L_\beta \cap \Gamma$ and $P_L^1(\beta)$ of $L_\beta \cap \partial\Xi$.

Let us first derive an expression for $P_L^0(\beta)$. Let $\mathcal{R}_0$ be the rose of directions of a single fibre Γ_0 defined for a Borel set $D \subseteq [0, \pi)$ as

$$\mathcal{R}_0(D) = \frac{E\nu_1\{x \in \Gamma_0 : \alpha(x) \in D\}}{E\nu_1(\Gamma_0)}.$$

Then, it is not difficult to see that $\mathcal{R} = \mathcal{R}_0$. Therefore, using (2),

$$P_L^0(\beta) = \lambda E\nu_1(\Gamma_0) \int_0^\pi |\sin(\alpha - \beta)| \mathcal{R}_0(d\alpha) = \lambda E h_\beta(\Gamma_0), \tag{3}$$

where $h_\beta(\Gamma_0)$ is the length of the projection of Γ_0 onto a line perpendicular to L_β.

Using Slivnyak's theorem (Stoyan *et al.*, 1995, p. 41), we find that the intensity of $L_\beta \cap \partial\Xi$ is

$$P_L^1(\beta) = (1 - p)\rho(\beta),$$

where p is the coverage probability

$$p = P(O \in \Xi) = 1 - \exp(-\lambda E\nu_2(\Xi_0))$$

and $\rho(\beta)$ is the intensity of $L_\beta \cap \cup_i (x_i + \partial\Xi_i)$,

$$\rho(\beta) = 2\lambda E h_\beta(\Xi_0),$$

see also Molchanov & Stoyan (1994, Theorem 3.1). Therefore, we get

$$P_L^1(\beta) = \exp(-\lambda E\nu_2(\Xi_0)) 2\lambda E h_\beta(\Xi_0). \tag{4}$$

Combining (3) and (4), we obtain the following relation between $P_L^0(\beta)$ and $P_L^1(\beta)$,

$$P_L^1(\beta) = \xi \xi_1(\beta) P_L^0(\beta), \tag{5}$$

where

$$\xi = 2\exp(-\lambda E\nu_2(\Xi_0)) \tag{6}$$

and

$$\xi_1(\beta) = \frac{E h_\beta(\Xi_0)}{E h_\beta(\Gamma_0)}. \tag{7}$$

Since $\xi_1(\beta)$ depends on the thickness of Ξ_0, we will call $\xi_1(\beta)$ a thickness factor. If $\Xi_0 = \Gamma_0$, we get

$$P_L^1(\beta) = 2P_L^0(\beta). \tag{8}$$

When the fibres Ξ_i's have some thickness, we cannot observe the central fibres Γ_i's and estimate their point intensity $P_L^0(\beta)$ on the sampling line L_β. Instead $\partial\Xi$ may be observable such that the intensity $P_L^1(\beta)$ of the point process $L_\beta \cap \partial\Xi$ can be estimated. If the extent of the fibres Ξ_i's is large compared to their thickness, then $\xi_1(\beta) \approx 1$ and the relation (5) can be regarded as approximately proportional

$$P_L^1(\beta) \approx \xi P_L^0(\beta) \tag{9}$$

with $0 < \xi < 2$. In such cases the rose of directions $\mathcal{R}$ can be estimated using the rose of intersections P_L^1 instead of P_L^0 without knowing the actual thickness of the fibres. Note also that if $\mathcal{R}$ is uniform, then $\xi_1(\beta)$ will be constant.

4 Examples of Boolean fibres

4.1 Circle-dilated segment model

The circle-dilated segment model is

$$\Xi_0 = \Gamma_0 \oplus B(O, r),$$

where the central fibre Γ_0 is a line segment with constant length l and orientation distribution $\mathcal{R}$, and $B(O, r)$ is a circular disc with centre O and radius r which determines the thickness of Ξ_0, see also Molchanov & Stoyan (1994).

Using this model, $L_A = \lambda l$,

$$\nu_2(\Xi_0) = 2lr + \pi r^2$$

and

$$Eh_\beta(\Xi_0) = \int_0^\pi (l|\sin(\alpha - \beta)| + 2r)\mathcal{R}(d\alpha).$$

Using (3) and (7), we find

$$\xi_1(\beta) = \frac{Eh_\beta(\Gamma_0) + 2r}{Eh_\beta(\Gamma_0)}$$

and, using (5),

$$P_L^1(\beta) = 2\exp(-\lambda(2lr + \pi r^2))(P_L^0(\beta) + 2r\lambda),$$

which is a linear function of $P_L^0(\beta)$. The proportionality can be supposed to hold if r is small compared to l. Note that under this assumption the intensity λ can be large and fibres overlap considerably. Under proportionality

$$P_L^1(\beta) \approx \xi P_L^0(\beta),$$

where $\xi = 2\exp(-\lambda(2lr + \pi r^2))$.

4.2 Elliptical segment model

The elliptical segment Ξ_0 is a very flat ellipse with a major axis of random length a and a minor axis of fixed length b. The length a follows the uniform distribution in (a_1, a_2) with mean value $\bar{a} = (a_1 + a_2)/2$. In this case the line segment Γ_0 has random length $l = 2a$ with mean value $\bar{l} = 2\bar{a}$. The length intensity of Γ is thereby $L_A = 2\lambda\bar{a}$. The orientation of Γ_0 follows the common orientation density $f_{\mathcal{R}}$. The elliptical segments are used in Figure 1.

Let us consider the formula (4) for the point intensity $P_L^1(\beta)$ of Ξ with an elliptical segment Ξ_0. At first we obtain

$$E\nu_2(\Xi_0) = \pi b\bar{a}$$

and from (6)

$$\xi = 2\exp(-\lambda\pi b\bar{a}).$$

The length of the projection of Ξ_0 onto the direction perpendicular to β is

$$h_\beta(\Xi_0) = 2\sqrt{a^2\sin^2(\beta - \alpha) + b^2\cos^2(\beta - \alpha)}$$

and the mean

$$Eh_\beta(\Xi_0) = \frac{2}{a_2 - a_1}\int_0^\pi I(a_1, a_2, b, \alpha, \beta)\mathcal{R}(d\alpha),$$

where

$$
\begin{aligned}
I(a_1, a_2, b, \alpha, \beta) &= \int_{a_1}^{a_2} \sqrt{a^2 \sin^2(\beta-\alpha) + b^2 \cos^2(\beta-\alpha)}\, da \\
&= |\sin(\beta-\alpha)| \int_{a_1}^{a_2} \sqrt{a^2 + b^2 \cot^2(\beta-\alpha)}\, da \\
&= |\sin(\beta-\alpha)| \frac{1}{2} [a_2 \sqrt{{a_2}^2 + b^2 \cot^2(\beta-\alpha)} \\
&\quad + b^2 \cot^2(\beta-\alpha) \log(a_2 + \sqrt{{a_2}^2 + b^2 \cot^2(\beta-\alpha)}) \\
&\quad - a_1 \sqrt{{a_1}^2 + b^2 \cot^2(\beta-\alpha)} \\
&\quad - b^2 \cot^2(\beta-\alpha) \log(a_1 + \sqrt{{a_1}^2 + b^2 \cot^2(\beta-\alpha)})].
\end{aligned}
$$

Using (4), we find

$$
P_L^1(\beta) = \frac{4\lambda \exp(-\lambda \pi b \bar{a})}{a_2 - a_1} \int_0^{\pi} I(a_1, a_2, b, \alpha, \beta) \mathcal{R}(d\alpha).
$$

The relation between $P_L^0(\beta)$ and $P_L^1(\beta)$ is not simple as for the circle-dilated segment model, but will be proportional if the fibres Ξ_i's are long compared to their thickness. In Table 1, the thickness factor

$$
\xi_1(\beta) = \frac{P_L^1(\beta)}{\xi P_L^0(\beta)}
$$

is shown for an elliptical segment model with $a_1 = 10$, $a_2 = 30$, $b = 1$ and $\lambda = 0.014$. The orientation distribution is the elliptic distribution with $(\tau, \kappa) = (1.178, 0.995)$, cf. (1). Note that in this example $\xi_1(\beta) \approx 1$ such that $P_L^0(\beta)$ and $P_L^1(\beta)$ can be regarded as proportional. At the same time, the overlap of the fibres is substantial. Thus, the coverage probability $p = 1 - \exp(-\lambda E \nu_2(\Xi_0)) = 0.585$ and the total area fraction of ellipses in the image $\lambda E \nu_2(\Xi_0) = 0.880$ differ. The overlap can also be seen in Figure 3b which shows a realization of the model. The example is treated in more detail in Section 7 below.

Table 1: The thickness factor $\xi_1(\beta)$ in eight directions for strong anisotropically distributed elliptical segments with $(\tau, \kappa) = (1.178, 0.995)$.

β	$\xi_1(\beta)$
0.000	1.002
0.464	1.004
0.785	1.008
1.107	1.020
1.571	1.008
2.034	1.003
2.356	1.002
2.678	1.002

5 From the point intensity $P_L^1(\beta)$ to the scaled variogram $V_L(d, \beta)$ in binary images

Let us consider a binary (0,1)-coloured image of Boolean fibres $\Xi \subset \mathbb{R}^2$ as a random function $Z(x) = 1_\Xi(x)$, $x \in \mathbb{R}^2$. In this section we examine the binary-valued function formed by the restriction of $Z(x)$ to the sampling line L_β. We consider the relation between the scaled variogram $V_L(d, \beta)$ and $P_L^1(\beta)$ observed on L_β. In Jeulin (2000) it is shown that $V_L(d, \beta)$ is approximately equal to $P_L^1(\beta)$, for small d. Below, we derive a refined relation.

Let $x, y \in \mathbb{R}^2$ be located on L_β at distance $d = ||x - y||$. The scaled variogram is defined as follows

$$V_L(d, \beta) = \frac{E|Z(x) - Z(y)|}{d}. \tag{10}$$

This quantity is equal to $2\gamma_1(d, \beta)/d$, where $\gamma_1(d, \beta)$ is the variogram of order 1 (Matheron, 1982). Note that the right-hand side of (10) only depends on d and β because of the stationary of Ξ. We get

$$\begin{aligned} E|Z(x) - Z(y)| &= 2P(x \in \Xi, y \notin \Xi) \\ &= 2[P(\Xi \cap \{y\} = \emptyset) - P(\Xi \cap \{x, y\} = \emptyset)]. \end{aligned}$$

For a Boolean model,

$$\begin{aligned} P(\Xi \cap \{y\} = \emptyset) &= \exp(-\lambda E\nu_2(\Xi_0 + \{y\})) \\ &= \exp(-\lambda E\nu_2(\Xi_0)) \end{aligned}$$

and

$$\begin{aligned} P(\Xi \cap \{x,y\} = \emptyset) &= \exp(-\lambda E\nu_2(\Xi_0 + \{x,y\})) \\ &= \exp(-\lambda E\nu_2(\Xi_0 \cup [\Xi_0 + \{y-x\}])). \end{aligned} \tag{11}$$

If d is small (as it is in our case), we can approximate in (11)

$$\nu_2(\Xi_0 \cup [\Xi_0 + \{y-x\}]) \approx \nu_2(\Xi_0) + dh_\beta(\Xi_0), \tag{12}$$

cf. e.g. Matheron (1975, p. 141). Thus

$$\begin{aligned} V_L(d,\beta) &= \frac{2[P(\Xi \cap \{y\} = \emptyset) - P(\Xi \cap \{x,y\} = \emptyset)]}{d} \\ &\approx \frac{2\exp(-\lambda E\nu_2(\Xi_0))(1 - \exp(-\lambda dEh_\beta(\Xi_0)))}{d} \\ &\overset{(*)}{\approx} \frac{2\exp(-\lambda E\nu_2(\Xi_0))\lambda dEh_\beta(\Xi_0)}{d} \\ &= P_L^1(\beta) \end{aligned} \tag{13}$$

for small d. At $(*)$ we have used

$$1 - \exp(-x) \approx x$$

for $x = \lambda dEh_\beta(\Xi_0)$.

A refined relation can be obtained if (12) is replaced by

$$\nu_2(\Xi_0 \cup [\Xi_0 + \{y-x\}]) \approx \nu_2(\Xi_0) + dh_\beta(\Xi_0) + d^2k_\beta(\Xi_0), \tag{14}$$

cf. Kiderlen & Jensen (2001). The coefficient $k_\beta(\Xi_0)$ seems not to have a simple geometric interpretation but satisfies

$$\frac{1}{2} \le k_\beta(\Xi_0) \le 1,$$

if Ξ_0 is r-smooth for some r (for all boundary points x of Ξ_0 there is a circular disc B_r with radius r such that $x \in B_r \subseteq \Xi_0$). Using (14) instead of (12), we find

$$V_L(d,\beta) \approx \frac{1 - \exp(-\lambda dEh_\beta(\Xi_0) - \lambda d^2Ek_\beta(\Xi_0))}{\lambda dEh_\beta(\Xi_0)} P_L^1(\beta). \tag{15}$$

In typical applications of our model $Eh_\beta(\Xi_0)$ is much larger than d. In such cases we can disregard the term $\lambda d^2 Ek_\beta(\Xi_0)$ in (15), since $\frac{1}{2} \leq Ek_\beta(\Xi_0) \leq 1$. Using the refined approximation

$$1 - \exp(-x) \approx x - \frac{x^2}{2}$$

for $x = \lambda d Eh_\beta(\Xi_0)$, we find from (15)

$$V_L(d,\beta) \approx \xi_2(d,\beta) P_L^1(\beta), \tag{16}$$

where

$$\begin{aligned} \xi_2(d,\beta) &= 1 - \frac{\lambda d Eh_\beta(\Xi_0)}{2} \\ &\overset{(**)}{=} 1 - \frac{d\xi_1(\beta) P_L^0(\beta)}{2}. \end{aligned}$$

We will call $\xi_2(d,\beta)$ a distance factor. At $(**)$ we have used (3) and (7).

Let us suppose that the thickness factor $\xi_1(\beta)$ is approximately 1 such that (9) holds. Then, we find

$$V_L(d,\beta) \approx \xi P_L^0(\beta) \tag{17}$$

for small d, cf. (13), and

$$V_L(d,\beta) \approx \xi \left(1 - \frac{d P_L^0(\beta)}{2}\right) P_L^0(\beta) \tag{18}$$

as a refined approximation, cf. (16). Recall that ξ is given in (6).

6 The scaled variogram $V_{L_{dl}}(d,\beta)$ observed in greyscale images

In cases where the observed image is a greyscale image, it is clearly of interest to develop procedures for estimating orientational characteristics which can be used without segmentation of the greyscale image into a binary image. This is indeed possible if the image can be modelled by a dead leaves random functions model with finite time t (Jeulin, 1989; 1993). This model generalizes earlier binary versions, cf. Matheron (1968) and Serra (1982).

The model is obtained by a sequential implantation of a random primary grey-valued grain at each point of a space-time Poisson point process, the more recent grains covering the already present grains. A typical application of the model concerns micrographs of stacked fibres seen from above.

Formally, a dead leaves random functions model can be constructed using a marked point process $\{[(x_i, t_i); \Phi_i]\}$ where $\{(x_i, t_i)\}$ is a homogeneous Poisson point process on $\mathbb{R}^2 \times [0, t]$ of intensity θ, say, and $\{\Phi_i\}$ are independent and identically distributed non-negative random functions on $\mathbb{R}^2$ which are independent of $\{(x_i, t_i)\}$. It is supposed that the support of Φ_i,

$$\Xi_i = \{x \in \mathbb{R}^2 : \Phi_i(x) > 0\},$$

is compact, see also Jeulin (1989). One can think of Φ_i as a primary grey-valued grain. We let Φ_0 and Ξ_0 be a typical random function and its support. The dead leaves random function $Z_t(x),\ x \in \mathbb{R}^2$, equals the grey value at x of the most recently arrived grain. To be more precise, let

$$I(x) = \{i : \Phi_i(x - x_i) > 0\}$$

be the set of primary grains hitting x. If $I(x)$ is empty, let $Z_t(x) = 0$. Otherwise, $Z_t(x) = \Phi_I(x - x_I)$ where I is the unique element in $I(x)$ such that $t_I > t_i$ for all $i \in I(x) \backslash \{I\}$.

Following Jeulin (2000), an expression for the scaled variogram

$$V_{L_{dl}}(d, \beta) = \frac{E|Z_t(x) - Z_t(y)|}{d}$$

can be derived where $x - y = d(\cos\beta, \sin\beta)$ as in the previous section, see also Matheron (1971, 1982). As previously, let $\Xi = \cup_{i=1}^{\infty}(x_i + \Xi_i)$ and let

$$\begin{aligned} q &= P(\Xi \cap \{y\} = \emptyset) \\ Q(d, \beta) &= P(\Xi \cap \{x, y\} = \emptyset). \end{aligned}$$

For the primary function and its support, let

$$\begin{aligned} r(d, \beta) &= E\nu_2(\Xi_0 \cap [\Xi_0 + \{y - x\}])/E\nu_2(\Xi_0) \\ \gamma_{1P}(d, \beta) &= \frac{1}{2}E|\Phi_0(x) - \Phi_0(y)|. \end{aligned}$$

Finally, let Z' be the grey value of a uniform random point on Ξ_0 where Ξ_0 is chosen to be area-weighted, i.e.

$$P(Z' \geq z) = \frac{E\nu_2(\{x \in \Xi_0 : \Phi_0(x) \geq z\}}{E\nu_2(\Xi_0)},\ z \geq 0.$$

Then, for small d,

$$V_{L_{dl}}(d,\beta) = 2(1-q)\gamma'_{1P}(0,\beta) - 2r'(0,\beta)[(1-q)2S - q\log q(EZ' - 2S)], \tag{19}$$

where

$$S = \int_0^\infty P(Z' \geq z)P(Z' < z)dz$$

given by Matheron (1982). The first term in (19) can be neglected for primary grains with slow variation of grey levels (low $\gamma'_{1P}(0,\beta)$). Since

$$P_L^1(\beta) \approx 2q\log q \cdot r'(0,\beta),$$

cf. (4) and (12), it follows that in such cases

$$V_{L_{dl}}(d,\beta) \approx \frac{-1}{q\log q}[(1-q)2S - q\log q(EZ' - 2S)]P_L^1(\beta) \tag{20}$$

for small d. Note that in the binary case $S = 0$ and $EZ' = 1$ such that (20) reduces to (13). If the thickness factor $\xi_1(\beta)$ of the fibres is close to 1, then it follows that $V_{L_{dl}}(d,\beta)$ is proportional to the intensity $P_L^0(\beta)$. Using various angles β, the rose of direction of the central fibres can thereby be estimated.

7 Simulation example

In order to illustrate the obtained results, we have performed a simulation study of the elliptical segment model. As in Section 4.2 the mean length of a central segment Γ_i is $\bar{l} = 40$ with major axis length a uniformly distributed in $(a_1, a_2) = (10, 30)$. The orientation distribution of Γ_i is uniform (the isotropic case) or an elliptic distribution with $(\tau, \kappa) = (1.178, 0.995)$ (the anisotropic case), cf. (1). The intensity of the points x_i is $\lambda = 0.014$. The length intensity of Γ is thereby $L_A = \lambda\bar{l} = 0.563$. Adding an ellipse to each Γ_i with minor axis length $b = 1$, the union of elliptical segments Ξ is obtained. Each realization of thick fibres Ξ is digitized into a (0,1)-valued image of size 250×200 where the background has a grey value zero (black) and the thick fibres have a grey value one (white). A pixel is coloured white if the centre of the pixel is covered by Ξ. A dead leaves model with finite time is used for colouring the binary image of thick fibres. In the greyscale image

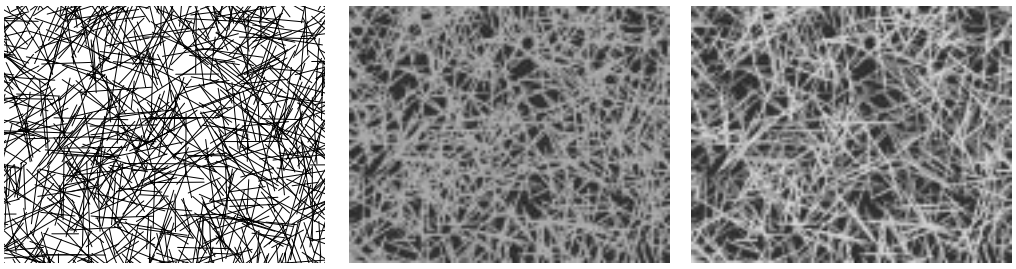

(a) (b) (c)

Figure 2: Realizations from three image models of isotropically distributed Boolean fibres with length intensity $L_A = 0.563$. (a) An image of line segments. (b) A digitized binary image of thick fibres. (c) A digitized dead leaves image of thick fibres.

the background has a value 50, the first third of $\{\Xi_i\}$ fallen on the image has grey value 150, the second 170 and the third 210. The grey value at a pixel is that of the most recent fibre. Note that this is an extension of the dead leaves random functions model described earlier since the Φ_i's are not identically distributed. All simulations have been carried out in an extended window in order to reduce edge-effects. The simulated images are shown in Figures 2 and 3 for the isotropic and the anisotropic case, respectively.

The point intensity and scaled variograms have been estimated in the four main directions: 0, $\pi/4 = 0.785$, $\pi/2 = 1.571$ and $3\pi/4 = 2.356$. Using a bundle of parallel sampling lines L_β, the point intensity is estimated from the image of line segments by

$$\hat{P}_L^0(\beta) = \frac{\#\{L_\beta \cap \Gamma\}}{\nu_1(L_\beta)},$$

for each direction, cf. e.g. Stoyan *et al.*, (1995). The scaled variograms are estimated from the digital images of Ξ by the unbiased estimator

$$\hat{V}_L(\beta) = \frac{\sum_{i=1}^{n} |Z(x_i) - Z(x_{i+1})|}{nd}, \tag{21}$$

where $x_1, ..., x_{n+1}$ are the pixel centres on the lines, $Z(x)$ is the grey value observed at x, and d is the distance between neighbour points,

$$d = ||x_i - x_{i+1}||, \ i = 1, ..., n.$$

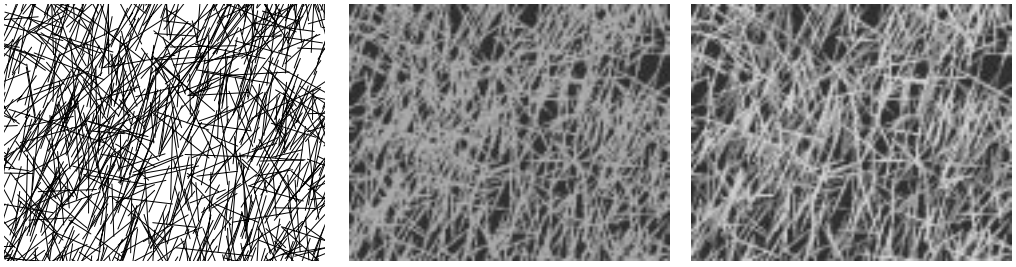

(a) (b) (c)

Figure 3: Realizations from three image models of anisotropically distributed Boolean fibres with orientation parameters $(\tau, \kappa) = (1.178, 0.995)$ and length intensity $L_A = 0.563$. (a) An image of line segments. (b) A digitized binary image of thick fibres. (c) A digitized dead leaves image of thick fibres.

For horizontal and vertical lines, $d = 1$, while for diagonal ones, $d = \sqrt{2}$. The estimated scaled variogram is denoted by $\hat{V}_{L_{bin}}(\beta)$ for the binary images and $\hat{V}_{L_{dl}}(\beta)$ for the dead leaves images. In Tables 2 and 3, the estimates are shown for the isotropic and anisotropic cases, respectively.

The ratio

$$\hat{\xi}(\beta) = \frac{\hat{V}_{L_{bin}}(\beta)}{\hat{P}_L^0(\beta)}$$

is constant if the approximation (17) is valid while

$$\hat{\xi}(d, \beta) = \frac{\hat{V}_{L_{bin}}(\beta)}{(1 - d\hat{P}_L^0(\beta)/2)\hat{P}_L^0(\beta)}$$

is constant if the refined approximation holds. The constant ξ of proportionality is in both cases

$$\xi = 2\exp(-\lambda E\nu_2(\Xi_0)) = 0.830.$$

According to Tables 2 and 3, it is clear that in this case the refined approximation is needed. The largest deviation of $\hat{\xi}(\beta)$ from ξ is seen in the directions where $d\hat{P}_L^0(\beta)$ is largest. Finally, it should be noticed that the ratios $\hat{V}_{L_{dl}}(\beta)/\hat{V}_{L_{bin}}(\beta)$ are fairly constant.

Table 2: In four directions the intensity $\hat{P}_L^0$ and the scaled variograms $\hat{V}_{L_{bin}}$ and $\hat{V}_{L_{dl}}$ estimated from Figures 2a, 2b and 2c, respectively, are shown together with the ratios $\hat{\xi}(\beta)$ and $\hat{\xi}(d,\beta)$. For details, see text.

β	d	$\hat{P}_L^0(\beta)$	$\hat{V}_{L_{bin}}(\beta)$	$\hat{V}_{L_{dl}}(\beta)$	$\hat{\xi}(\beta)$	$\hat{\xi}(d,\beta)$
0.000	1	0.355	0.251	36.26	0.707	0.860
0.785	$\sqrt{2}$	0.347	0.223	32.67	0.643	0.852
1.571	1	0.347	0.244	34.84	0.703	0.851
2.356	$\sqrt{2}$	0.357	0.230	33.09	0.644	0.862

Table 3: In four directions the intensity $\hat{P}_L^0$ and the scaled variograms $\hat{V}_{L_{bin}}$ and $\hat{V}_{L_{dl}}$ estimated from Figures 3a, 3b and 3c, respectively, are shown together with the ratios $\hat{\xi}(\beta)$ and $\hat{\xi}(d,\beta)$. For details, see text.

β	d	$\hat{P}_L^0(\beta)$	$\hat{V}_{L_{bin}}(\beta)$	$\hat{V}_{L_{dl}}(\beta)$	$\hat{\xi}(\beta)$	$\hat{\xi}(d,\beta)$
0.000	1	0.446	0.285	41.56	0.639	0.822
0.785	$\sqrt{2}$	0.294	0.193	28.19	0.656	0.829
1.571	1	0.280	0.199	28.23	0.711	0.826
2.356	$\sqrt{2}$	0.436	0.253	36.98	0.580	0.839

8 Further comments on digitization

In this section the problem of estimating the scaled variogram from observations on digital lines instead of continuous lines is shortly discussed. We concentrate on the four intermediate directions $\beta = 0.464,\ 1.107,\ 2.034,\ 2.678$ between the four main directions $\beta = 0,\ \pi/4,\ \pi/2,\ 3\pi/4$.

A digital line $\bar{L}_\beta$ in the intermediate direction β is often chosen as a chain of 8-connected pixels. The neighbour points of the sequence $x_1, ..., x_{n+1}$ on $\bar{L}_\beta$ are located in two angularly adjacent main directions β_1 and β_2 and at two distances d_1 and d_2, respectively, see Table 4. Let us for simplicity assume that n is even, $n = 2k$, and that $||x_{2j-1} - x_{2j}|| = d_1$ in a direction β_1 and $||x_{2j} - x_{2j+1}|| = d_2$ in a direction β_2, $j = 1, ..., k$. Then the straightforward

estimator of the scaled variogram is

$$\hat{V}_L(\beta) = \frac{\sum_{i=1}^{n} |Z(x_i) - Z(x_{i+1})|}{k(d_1 + d_2)} \tag{22}$$

for a digital image, compare with (21). However, the mean is, in the binary case, a weighted average of $V_L(d_1, \beta_1)$ and $V_L(d_2, \beta_2)$

$$E\hat{V}_{L_{bin}}(\beta) = \frac{d_1}{d_1 + d_2} V_L(d_1, \beta_1) + \frac{d_2}{d_1 + d_2} V_L(d_2, \beta_2).$$

For instance, if $\beta = \arctan(1/2) = 0.464$, the mean is a weighted average of $V_L(1, 0)$ and $V_L(\sqrt{2}, \pi/4)$

$$E\hat{V}_{L_{bin}}(0.464) = \frac{1}{1 + \sqrt{2}} V_L(1, 0) + \frac{\sqrt{2}}{1 + \sqrt{2}} V_L(\sqrt{2}, \pi/4).$$

Correspondingly, in the greyscale case $E\hat{V}_{L_{dl}}(\beta)$ is a weighted average of $V_{L_{dl}}(d_1, \beta_1)$ and $V_{L_{dl}}(d_2, \beta_2)$. The mean is thus not equal to $V_L(d, \beta)$ or $V_{L_{dl}}(d, \beta)$ for some suitably chosen d, as might be expected at first hand. An alternative choise is to use every second pixel of the sequence $x_1, ..., x_{n+1}$ such that the distance d between points becomes $\sqrt{5}$. Then the unbiased estimator (21) can be employed instead of (22). In order to use the approximations derived in this paper, it is, however, required that d is small.

Table 4: The values of the parameters β_1, d_1, β_2, d_2 for each intermediate direction β.

β	β_1	d_1	β_2	d_2
0.464	0	1	$\frac{\pi}{4}$	$\sqrt{2}$
1.107	$\frac{\pi}{4}$	$\sqrt{2}$	$\frac{\pi}{2}$	1
2.034	$\frac{\pi}{2}$	1	$\frac{3\pi}{4}$	$\sqrt{2}$
2.678	$\frac{3\pi}{4}$	$\sqrt{2}$	0	1

9 Conclusion

The aim of this study has been to make stereological inference on the orientation of unobservable central Boolean fibres from observations made on

thickened fibres in digital images. In the paper we have documented that this is indeed possible under regularity conditions. First of all, the relation between the roses of intersections P_L^0 and P_L^1, where P_L^0 refers to central fibres and P_L^1 to the boundary of the union of the thick fibres, is proportional if the extent of thick fibres is large compared to their thickness. In such cases the actual thickness and overlap of fibres are not important. Secondly, the scaled variogram $V_L(d, \beta)$ calculated from a digital binary image approximates $P_L^1(\beta)$ if the resolution of the grid is high. Under these assumptions the point intensity $P_L^0(\beta)$ can thereby be estimated up to a constant factor directly from the scaled variogram, which is easy and fast to determine. These results also hold for multicoloured fibres modelled by a dead leaves random functions model. For a binary image which has been digitized with a grid of low resolution the refined approximation between $V_L(d, \beta)$ and $P_L^1(\beta)$ can be used. The same is true for a greyscale image if segmentation into a binary image is possible.

10 Acknowledgements

We would like to express our gratitude to Adrian Baddeley and Markus Kiderlen for discussion and suggestions. The financial support from the MaDaMe Program of the Academy of Finland (n:o 50139), NorFA (n:o 000519) and MaPhySto, Centre for Mathematical Physics and Stochastics funded by a grant from the Danish National Research Foundation, is appreciated.

References

Erkkilä, A.-L., Pakarinen, P. & Odell, M., (1998): Sheet forming studies using layered orientation analysis. *Pulp Paper Canad.*, **99**, T39–T43.

Forgacs, O. L. & Strelis, J., (1963): The measurement of the quantity and orientation of chemical pulp fibres in the surfaces of newsprint. *Pulp Paper Mag. Canad.*, **64**, T3–T13.

Hilliard, J. E., (1962): Specification and measurement of microstructural anisotropy. *Trans. Metall. Soc. Am. Inst. Metall. Eng.*, **224**, 1201–1211.

Jeulin, D., (1989): Morphological modeling of images by sequential random functions. *Signal Processing*, **16**, 403–431.

Jeulin, D., (1993): Random models for morphological analysis of powders. *J. Microsc.*, **172**, 13–21.

Jeulin, D., (2000): Variograms of the dead leaves model. Research Report N-31/00/MM, *Paris School of Mines Publication.*

Kiderlen, M. & Jensen, E. B. V., (2001): The directional distribution of planar digitized Boolean models. Research report, Laboratory for Computational Stochastics, University of Aarhus. In preparation.

Matheron, G., (1967): *Eléments pour une Théorie des Milieux Poreux*. Masson, Paris.

Matheron, G., (1968): Schéma booléen séquential de partition aléatoire. Research Report N-83 CMM, *Paris School of Mines Publication.*

Matheron, G., (1971): The theory of regionalized variables and its applications. Cahiers du Centre de Morphologie Mathématique Vol. 5, 211 pp., *Paris School of Mines Publication.*

Matheron, G., (1972): Ensembles fermés aleátoires, ensembles semi-Markoviens et polyèdres poissoniens. *Adv. App. Prob.*, **4**, 508–541.

Matheron, G., (1975): *Random Sets and Integral Geometry*. John Wiley and Sons, New York.

Matheron, G., (1982): La destructuration des hautes teneurs et le krigeage des indicatrices. Research Report N-761/82/G, *Paris School of Mines Publication.*

Matthes, K., (1963): Stationäre zufällige Punktfolgen. *Jahresbericht Deutsche Math. Verein.*, **66**, 66–79.

Mecke, J., (1981): Formulas for stationary planar fibre processes III – intersections with fibre systems. *Math. Operationsforsch. Statist., Ser. Statistics*, **12**, 201–210.

Mecke, J. & Stoyan, D., (1980): Formulas for stationary planar fibre processes I – general theory. *Math. Operationsf. Statist., Ser. Statistics*, **11**, 267–279.

Molchanov, I. & Stoyan, D., (1994): Directional analysis of fibre processes related to Boolean models. *Metrika*, **41**, 183–199.

Serra, J., (1982): *Image Analysis and Mathematical Morphology*. Academic Press, London.

Stoyan, D., Kendall, W. S. & Mecke, J., (1995): *Stochastic Geometry and its Applications*. Wiley, New York, 2nd edition.